Multiregional tumor drug-uptake imaging by PET and microvascular morphology

in end-stage diffuse intrinsic pontine glioma

Sophie E.M. Veldhuijzen van Zanten[1,2], A. Charlotte P. Sewing[1,2*], Arthur van Lingen[3], Otto S. Hoekstra[3], Pieter Wesseling[2,4,5], Michaël H. Meel[1,2], Dannis G. van Vuurden[1,2], Gertjan J.L. Kaspers[1,6], Esther Hulleman[1,2], Marianna Bugiani[4]*

[1]*Dep. Pediatrics, Division of Oncology/Haematology, VUmc, Amsterdam, The Netherlands*
[2]*Neuro-oncology Research Group, Cancer Center Amsterdam, VUmc, The Netherlands*
[3]*Dep. Radiology and Nuclear Medicine, VUmc, Amsterdam, The Netherlands*
[4]*Dep. Pathology, VUmc, Amsterdam, The Netherlands*
[5]*Dep. Pathology, Princess Máxima Center for Pediatric Oncology, Utrecht, The Netherlands*
[6] *Dep. Pediatrics, Princess Máxima Center for Pediatric Oncology, Utrecht, The Netherlands.*
[*] Equal contribution

Running head

Drug-uptake and tumor morphology in DIPG

First and corresponding author

Sophie E.M. Veldhuijzen van Zanten

VU University Medical Center, Dep. Pediatrics, Div. Oncology/Hematology

De Boelelaan 1118, 1081HZ Amsterdam, The Netherlands

T/ +31-648472180

F/ +31-204440849

E/ s.veldhuijzen@vumc.nl

Word count

2528

ABSTRACT

Inadequate tumor uptake of the vascular endothelial growth factor (VEGF) antibody bevacizumab could explain lack of effect in diffuse intrinsic pontine glioma (DIPG). **Methods:** By combining data from a positron emission tomography (PET) imaging study using zirconium-89(^{89}Zr)-labeled bevacizumab and an autopsy study, a 1-on-1 analysis of multiregional *in vivo* and *ex vivo* ^{89}Zr-bevacizumab uptake, tumor histology and vascular morphology in a DIPG patient was performed. **Results:** *In vivo* ^{89}Zr-bevacizumab measurements showed heterogeneity between lesions. Additional *ex vivo* measurements and immunohistochemistry of cervicomedullary metastasis samples, showed highest uptake in the area with marked microvascular proliferation. In the primary pontine tumor all samples showed similar vascular morphology. Other histological features were similar between samples studied. **Conclusion:** *In vivo* bevacizumab-PET serves to identify heterogeneous uptake between tumor lesions, while subcentimeter intra-lesional heterogeneity could only be identified by *ex vivo* measurements. Bevacizumab uptake is enhanced by vascular proliferation, although our results suggest it is not the only determinant of intra-lesional uptake heterogeneity.

Key words

Brain stem neoplasm, PET, ^{89}Zr-bevacizumab, microvascular morphology, VEGF

INTRODUCTION

End-stage DIPG shows glioblastoma histology[1] and overexpression of proangiogenic factors, including VEGF[1,2]. Whether DIPG patients benefit from anti-VEGF treatment, such as the monoclonal antibody bevacizumab, however, is still unclear[3–5]. So far, results of trials with bevacizumab have been disappointing[6,7]. A recent drug imaging study assessing tumor uptake of zirconium-89(^{89}Zr)-labeled bevacizumab in DIPG[8] showed inter and intra-patient heterogeneity, but factors determining uptake are currently unknown.[9] Therefore, this study aims to perform a 1-on-1 analysis of multiregional *in vivo* and *ex vivo* ^{89}Zr-bevacizumab uptake, tumor histology and vascular morphology in a DIPG patient.

MATERIALS AND METHODS

A 12-year old female patient presented with a left abducens nerve paralysis. Brain MR-imaging revealed a T1-weighted hypointense, T2-weighted hyperintense lesion infiltrating over 50% of the pons[10] suggestive of DIPG. Biopsy demonstrated high-grade diffuse glioma features, and Sangers sequencing of *H3F3A* and *HIST1H3B* revealed a wild-type status[11]. Whole exome sequencing showed no mutations in HIST1H3C or HIST2H3C either. A diagnosis of Histone H3 wild-type DIPG was made[12]. The patient was enrolled in the DIPG study VUmc-01 (Dutch Trial Register: NTR2391) - phase A, and treated with radiotherapy (30x1.8=54Gy) and weekly gemcitabine (175mg/m^2/week) for six weeks. Progression-free survival was 3.8 months. After disease progression, the patient participated in a molecular imaging study (NTR3518), including an immuno-PET scan at 145 hours postinjection of 0.1mg/kg bevacizumab labeled with 0.9MBq/kg zirconium-89, as described[9]. Four days afterwards, the patient died (death was unrelated to study participation) and participated in an autopsy study. All three studies were approved by the Institutional Review Board of VU University Medical Center and performed in accordance with the Declaration of Helsinki. For each study, both parents gave written informed consent.[9,13]

In vivo ^{89}Zr-bevacizumab Uptake Measurements

In vivo ^{89}Zr-bevacizumab uptake was quantified as decay-corrected maximum activity concentration (corr. ACmax in Bq/mL) in manually delineated volumes of interest, i.e. tumor areas with visually enhanced uptake. Activity concentrations were also converted into Standardized Uptake Values (SUVs), i.e. decay-

corrected maximum activity concentration normalized to injected dose/body weight.

Ex vivo [89]Zr-bevacizumab Uptake Measurements

Brain autopsy was performed 2 hours post-mortem. Multiple 0.5 cm^3 tumor and control samples (macroscopically non-affected brain, cerebrospinal fluid (CSF) and blood) were obtained for *ex vivo* [89]Zr-radioactivity measurements and histological analysis. *Ex vivo* radioactivity concentrations were measured with a gamma well counter (Wallac 1480 Wizard, Turku, Finland). The *in vivo* PET scanner (Philips Ingenuity TF-128 PET-CT-scanner, *Philips Healthcare*) was cross-calibrated with the well counter[14,15]. *Ex vivo* [89]Zr-radioactivity concentrations were also quantified as corr. ACmax and converted into SUV.

Immunohistochemistry

Four-µm-thick formalin-fixed, paraffin-embedded tissue sections were stained with Hematoxylin&Eosin (H&E) and immunostained as previously validated and described[16,17] against glial fibrillary acidic protein (GFAP; Dako, 1:400); MIB-1 (Dako, 1:40); GLUT-1 (Thermo Scientific, 1:200), smooth muscle actin (SMA, Dako, 1:200), collagen-IV (Dako, 1:50), CD34 (Dako, 1:50) and VEGF (Pharamgen, 1:50). Specific stainings were chosen to determine differences in proliferation grade in the tumor in vascular endothelial cells (MIB-1), to highlight vascular morphology by identifying endothelial cells (CD34), vascular smooth muscle cells and activated pericytes (SMA) and the vascular basal membrane (Coll-IV), to visualize tumor morphology and resident astrocytes (GFAP), to identify blood brain barrier integrity and areas of increased hypoxia (GLUT1), and to determine VEGF expression (VEGF). Immunopositivity was detected with 3,3'-Diaminobenzidine (DAB). Omitting primary antibodies yielded no significant staining. Sections were photographed using a Leica DM6000B microscope.

RESULTS

In vivo [89]Zr-bevacizumab Uptake

The T1 post-gadolinium-MR-images obtained eight days pre-mortem showed a 3.6x3.3cm primary pontine tumor, with strong contrast enhancement but no apparent necrosis. Furthermore, extensive meningeal and subependymal metastases in the right ventricular trigone (VTM) and cervicomedullary junction (CMM)

(Fig. 1), as well as in the right frontal lobe, left Sylvian fissure, left lateral ventricle posterior horn, and along the spinal cord were observed (Supplemental Figs. 1A-F). At t=145 the most intense ^{89}Zr-bevacizumab uptake-positivity was seen in the CMM (corr. ACmax 7800Bq/mL, SUV 9.9, volume 2.0mL), followed by the primary pontine tumor (5607Bq/mL, SUV 7.1, 13.1mL) and the VTM (2537Bq/mL, SUV 3.2, 1.2mL).

Ex vivo ^{89}Zr-bevacizumab Uptake

Ex vivo radioactivity measurements at t=242 were performed in multiple tumor samples (Fig. 2A), including the VTM, primary tumor, CMM, and a small 0.02gram fragment of dural metastasis that was previously undetected by MRI and PET (Supplemental Fig. 2), and macroscopically normal areas of the pons, cerebellum and dura. Tracer uptake was highest in the dural metastasis (22652Bq/mL, SUV 28.7) and CMM samples, with considerable difference between the cranial (27152Bq/mL, SUV 34.4) and caudal (16184Bq/mL, SUV 20.5) part. Differences in uptake were also observed between the cranial (2949Bq/mL, SUV 3.7) and caudal (11343Bq/mL, SUV 14.4) part of the primary tumor. Radioactivity was low in normal tissue samples (<1844Bq/mL, SUV <2.3), CSF (62Bq/mL, SUV 0.1) and blood (716Bq/mL, SUV 0.9).

Correlation Between *In vivo* and *Ex vivo* ^{89}Zr-bevacizumab Uptake

Fig. 2B shows the ratio between *in vivo* and *ex vivo* ^{89}Zr-bevacizumab uptake of the primary tumor, VTM and CMM.

Correlation Between *Ex vivo* ^{89}Zr-bevacizumab Uptake and Histology

After *ex vivo* radioactivity measurements, multiple samples from the primary tumor and CMM were investigated with (immuno)histochemistry to explore differences in histology as possible explanation for tracer uptake heterogeneity. H&E showed diffuse growth pattern, high cellularity and variable cytonuclear atypia (Figs. 3A and 3B) in all tumor samples, and confirmed absence of tumor in macroscopically normal tissue. Necrosis and florid glomeruloid microvascular proliferation were only present in the cranial CMM (with highest *ex vivo* radioactivity) (Fig. 3A). In this sample, MIB-1 staining was positive in up to 50% of tumor cells and in numerous (endothelial) cells in the microvascular walls (Fig. 3B). In the remaining

samples microvascular proliferation was less pronounced: here, 30% (in both primary tumor samples) to 50% (in the caudal CMM sample) of tumor cell nuclei were MIB-1-positive, whereas endothelial cells were MIB-1-negative (Fig. 3B). GFAP was expressed in tumor cells in the primary tumor and CMM, as well as in residual non-neoplastic astrocytes (Fig. 3C). Staining of CD34 showed partial loss of microvascular immunoreactivity in the caudal part of the primary tumor. In the other samples, CD34-immunopositivity was maintained (Fig. 3D). Immunoreactivity for GLUT-1 was similar in all samples (Fig. 3E). Staining of collagen-IV and SMA highlighted the vascular basal lamina and tunica media, respectively, in all samples without obvious differences (Fig. 3E). Staining of VEGF was similar amongst all samples (Fig. 3F).

DISCUSSION

This study directly correlates multiregional [89]Zr-bevacizumab uptake to tumor histology and vascular morphology in a patient with histone H3 wild-type DIPG[12]. Observed differences between *in vivo* and *ex vivo* radioactivity measurements reflect tracer pharmacokinetics, e.g. ongoing tracer clearance from blood over time, in combination with spatially and/or temporally heterogeneously increasing bevacizumab tissue deposition. Moreover, *in vivo* PET underestimates true activity in small lesions (in this case the CMM and VTM) because of partial volume effects. Due to this effect[14], the actual radioactivity concentration as assessed by imaging at t=145 post-[89]Zr-bevacizumab injection was likely underestimated by circa 70%. Finally, as opposed to *ex vivo* measurements, at t=145 intravascular [89]Zr-bevacizumab still contributes to the *in vivo* PET tumor signal (blood pool SUV~4)[9]. Thus, where *in vivo* PET serves to identify whole body tracer distribution and heterogeneity between lesions, subcentimeter intra-lesional heterogeneity of tracer distribution can only be defined with *ex vivo* measurements.

Interestingly, H&E and MIB-1 staining showed prominent microvascular proliferation in the cranial part of the CMM, with higher [89]Zr-bevacizumab uptake, versus the caudal part with lower uptake. No other histological differences were found between the two samples, such as pattern of tumor growth, extent of necrosis or different immunoreactivity for endothelial markers. In the two samples from the pons, intra-lesional uptake heterogeneity was also observed, although here both areas showed similar vascular

morphology, tumor growth, and extent of necrosis. These findings suggest that vascular proliferation is an important, yet not the only determinant of intra-lesional heterogeneity in bevacizumab uptake.

The presence of microvascular proliferation and disorganized vessels[18] in WHO grade IV glioma is considered a consequence of hypoxia-induced overexpression of proangiogenic factors, including VEGF[1,2]. In the cranial CMM sample, glomeruloid microvascular structures with increased endothelial cell turnover (as determined by MIB-1-immunoreactivity) were prominent. Based on this, VEGF was expected to be overexpressed. VEGF immunoreactivity, however, showed mostly aspecific staining and did not differ between samples. This may be explained by the very short half-life of the VEGF protein (15-20 minutes[19]) being incompatible with its immunohistochemical detection two hours post-mortem. Glut-1 staining was similar in all samples analyzed, suggesting a partially intact blood-brain barrier (BBB). However, our histological analysis did not provide definitive clues to determine the role of BBB integrity in bevacizumab uptake in this case.

CONCLUSION

Although concerning a single case, we conclude that *in vivo* PET is capable of detecting heterogeneity in bevacizumab uptake between lesions, which correlates well to *ex vivo* measurements. However, PET cannot detect subcentimeter intra-lesional uptake heterogeneity. Furthermore, our results suggest that targeting of bevacizumab is enhanced in areas with vascular proliferation. However, as significant inter- and intra-lesional heterogeneity was also observed in areas that did not show differences in vascular proliferation, other factors present in the DIPG microenvironment likely also play a role. Because the DIPG microenvironment is heterogeneous and dynamic in nature[3], patients are likely to fail treatment if timing and patient selection are not optimized. The results of this study underline the potential of immuno-PET studies, especially when combined with biopsy or/and autopsy studies, in the quest for optimal selection and timing of treatment schedules.

Financial disclosure

None

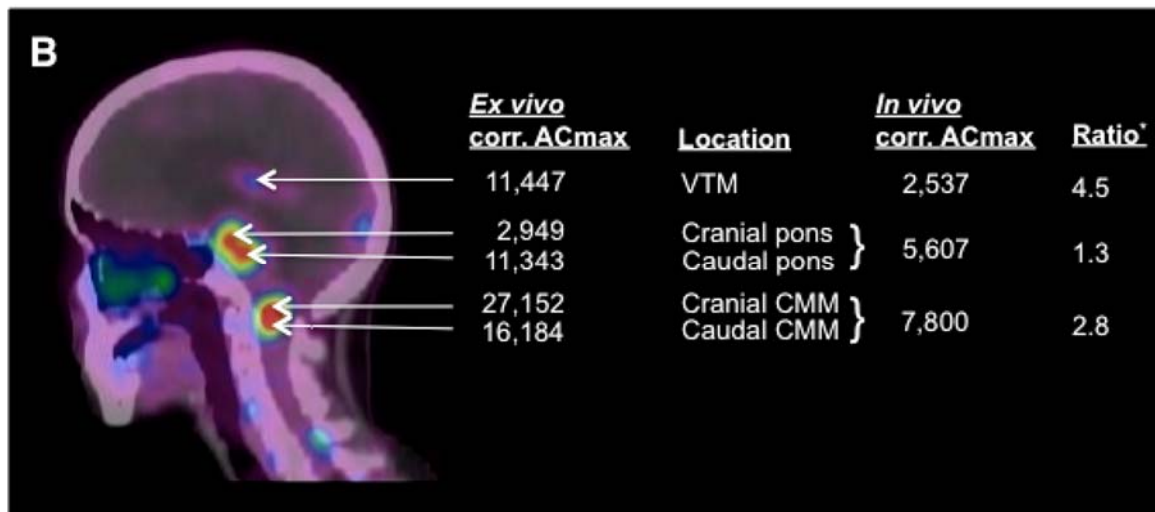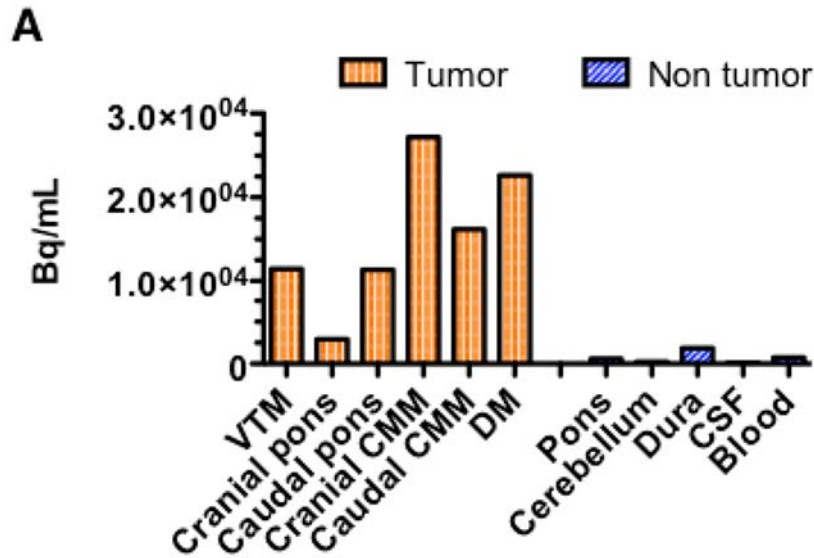**Acknowledgements**

REFERENCES

1.   Buczkowicz P, Bartels U, Bouffet E, Becher O, Hawkins C. Histopathological spectrum of paediatric diffuse intrinsic pontine glioma: diagnostic and therapeutic implications. *Acta Neuropathol.* 2014;128:573-81.

2.   Puget S, Philippe C, Bax DA, et al. Mesenchymal transition and PDGFRA amplification/mutation are key distinct oncogenic events in pediatric diffuse intrinsic pontine gliomas. *PLoS One.* 2012;7:e30313.

3.   Ballester LY, Wang Z, Shandilya S, et al. Morphologic characteristics and immunohistochemical profile of diffuse intrinsic pontine gliomas. *Am J Surg Pathol.* 2013;37:1357-64.

4.   Gururangan S, Chi SN, Young Poussaint T, et al. Lack of efficacy of bevacizumab plus irinotecan in children with recurrent malignant glioma and diffuse brainstem glioma: a Pediatric Brain Tumor Consortium study. *J Clin Oncol.* 2010;28:3069-3075.

5.   Jansen MHA, Lagerweij T, Sewing ACP, et al. Bevacizumab targeting diffuse intrinsic pontine glioma: results of 89Zr-bevacizumab PET imaging in brain tumor models. *Mol Cancer Ther.* 2016;15:2166-74.

6.   Parekh C, Jubran R, Erdreich-Epstein A, et al. Treatment of children with recurrent high grade gliomas with a bevacizumab containing regimen. *J Neurooncol.* 2011;103:673-80.

7.   Zaky W, Wellner M, Brown RJ, Blüml S, Finlay JL, Dhall G. Treatment of children with diffuse intrinsic pontine gliomas with chemoradiotherapy followed by a combination of temozolomide, irinotecan, and bevacizumab. *Pediatr Hematol Oncol.* 2013;30:623-32.

8.   Veldhuijzen van Zanten S, Jansen M, van Vuurden D, et al. Molecular drug imaging: pioneering work in children with diffuse intrinsic pontine glioma. *Neuro Oncol.* 2014;16(suppl 1):i40-i59.

9.   Jansen M, Veldhuijzen van Zanten SE, Van Vuurden DG, et al. Molecular Drug Imaging: 89Zr-bevacizumab PET in Children with Diffuse Intrinsic Pontine Glioma. *J Nucl Med.* 2016;5:711-716.

10.   Barkovich AJ, Krischer J, Kun LE, et al. Brain stem gliomas: a classification system based on magnetic resonance imaging. *Pediatr Neurosurg.* 1990;16:73-83.

11.   Wu G, Broniscer A, McEachron TA, et al. Somatic histone H3 alterations in pediatric diffuse intrinsic pontine gliomas and non-brainstem glioblastomas. *Nat Genet.* 2012;44:251-3.

12. Louis DN, Perry A, Reifenberger G, et al. The 2016 World Health Organization classification of tumors of the central nervous system: a summary. *Acta Neuropathol.* 2016;131:803-20.

13. Caretti V, Jansen MHA, van Vuurden DG, et al. Implementation of a multi-institutional diffuse intrinsic pontine glioma autopsy protocol and characterization of a primary cell culture. *Neuropathol Appl Neurobiol.* 2013;39:426-36.

14. Makris NE, Boellaard R, Visser EP, et al. Multicenter harmonization of 89Zr PET/CT performance. *J Nucl Med.* 2014;55:264-7.

15. Greuter HNJM, Boellaard R, van Lingen A, Franssen EJF, Lammertsma AA. Measurement of 18F-FDG concentrations in blood samples: comparison of direct calibration and standard solution methods. *J Nucl Med Technol.* 2003;31:206-9.

16. Kevelam SH, Bugiani M, Salomons GS, et al. Exome sequencing reveals mutated SLC19A3 in patients with an early-infantile, lethal encephalopathy. *Brain.* 2013;136:1534-43.

17. Navis AC, Hamans BC, Claes A, et al. Effects of targeting the VEGF and PDGF pathways in diffuse orthotopic glioma models. *J Pathol.* 2011;223:626-34.

18. Michiel Wagemakers. Angiogenesis and Angiopoietins in Human Gliomas. *University of Groningen* 2015;Chapter 2:23-44

19. Levy NS, Chung S, Furneaux H, Levy AP. Hypoxic stabilization of vascular endothelial growth factor mRNA by the RNA-binding protein HuR. *J Biol Chem.* 1998;273:6417-23.

FIGURE LEGENDS
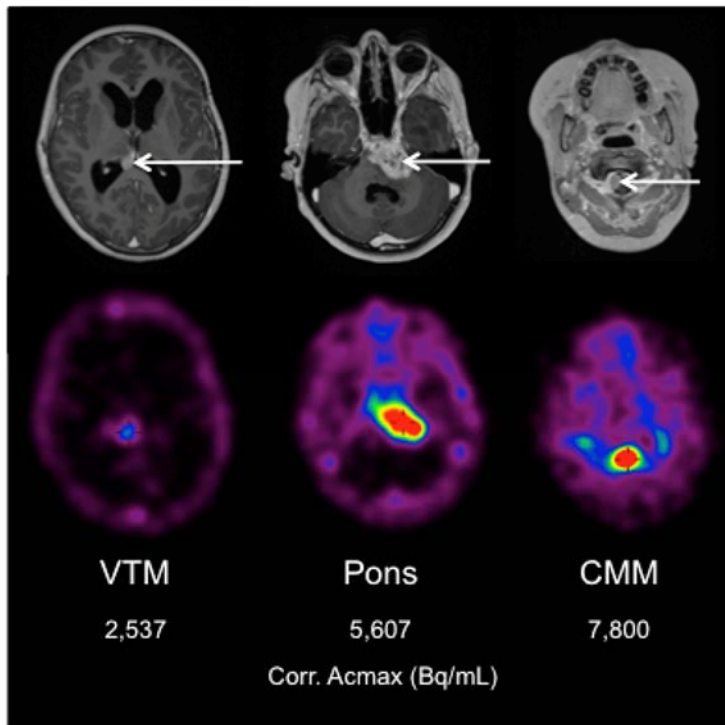
Figure 1. Gadolinium-enhanced T1-MR-images obtained 8 days before death and corresponding PET slices obtained 4 days before death (t=145 post-^{89}Zr-bevacizumab-injection) showing the primary pontine tumor, and metastases in the right ventricular trigone (VTM) and cervicomedullary junction (CMM). White arrows represent areas of disease.
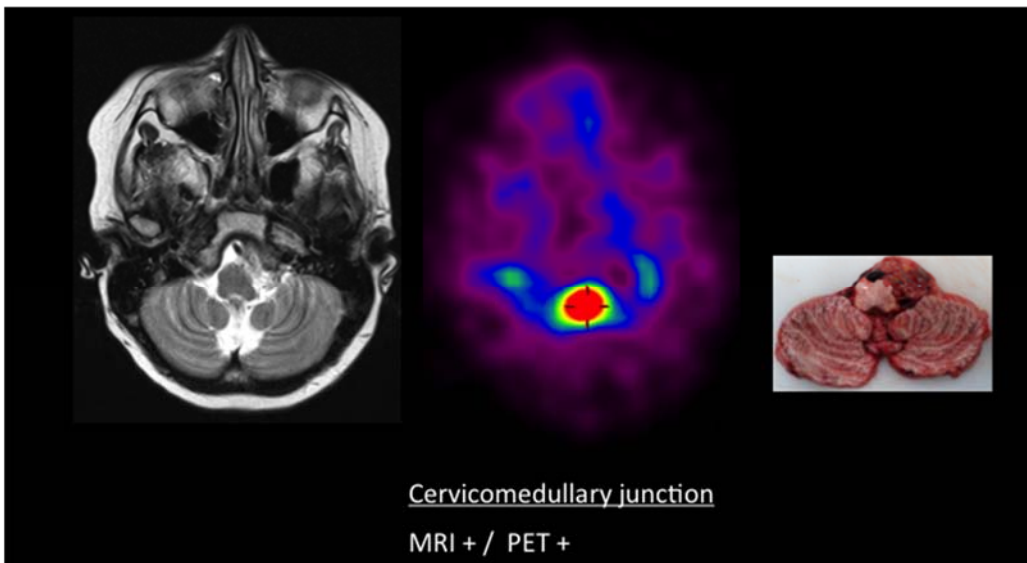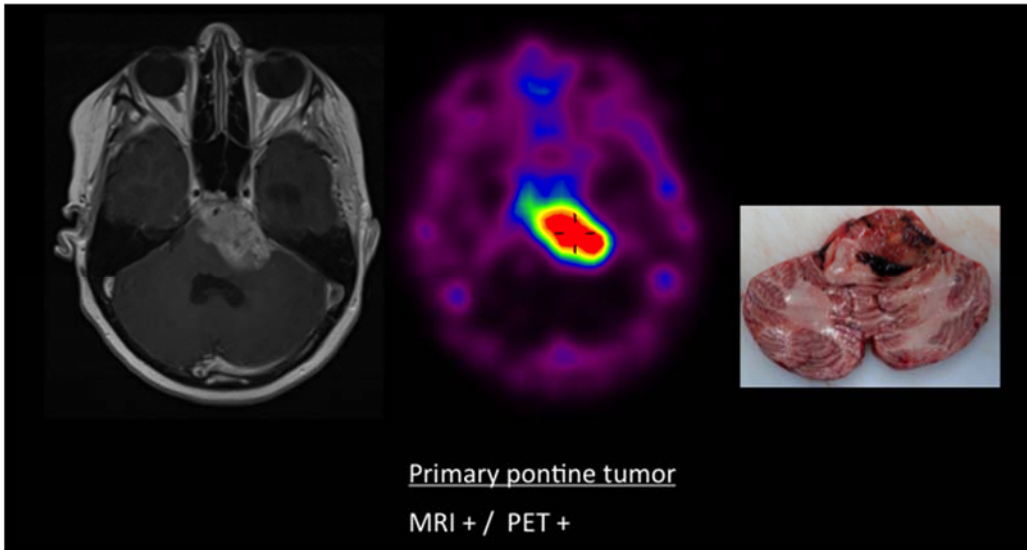
A

B

Ex vivo corr. ACmax	Location	In vivo corr. ACmax	Ratio*
11,447	VTM	2,537	4.5
2,949	Cranial pons		
11,343	Caudal pons }	5,607	1.3
27,152	Cranial CMM		
16,184	Caudal CMM }	7,800	2.8

Figure 2(A). *Ex vivo* [89]Zr-bevacizumab uptake (t=242 p.i.) in tumor samples (orange) and macroscopically normal tissue samples, CSF and blood (blue), **(B)** correlated to *in vivo* [89]Zr-bevacizumab uptake (white arrows, t=145 p.i.,). Ventricular trigone metastasis (VTM), cervicomedullary metastasis (CMM), dural metastasis (DM), cerebrospinal fluid (CSF). *The numerator for ex vivo uptake of the primary tumor and CMM is the average of the cranial and caudal corr. ACmax.
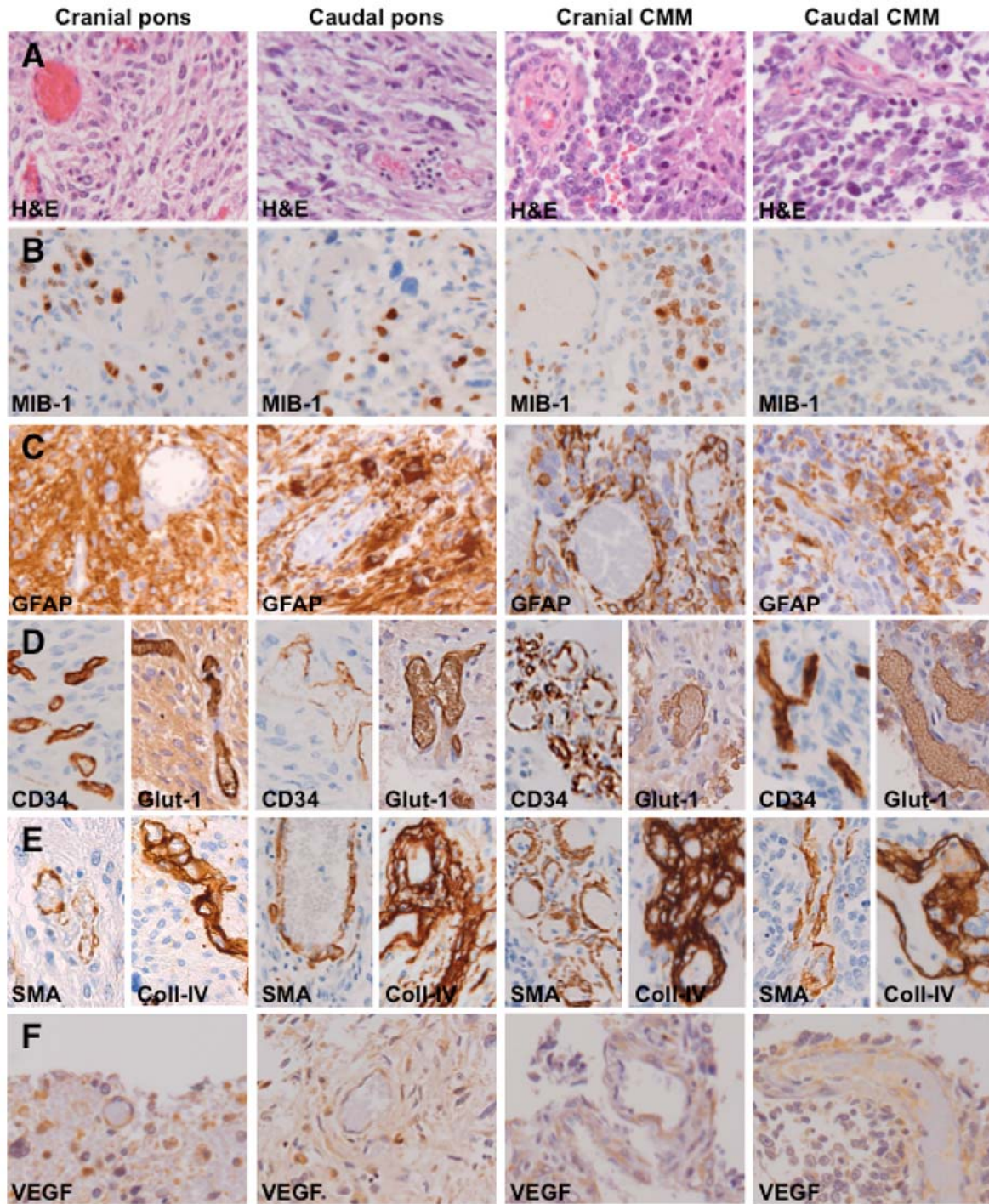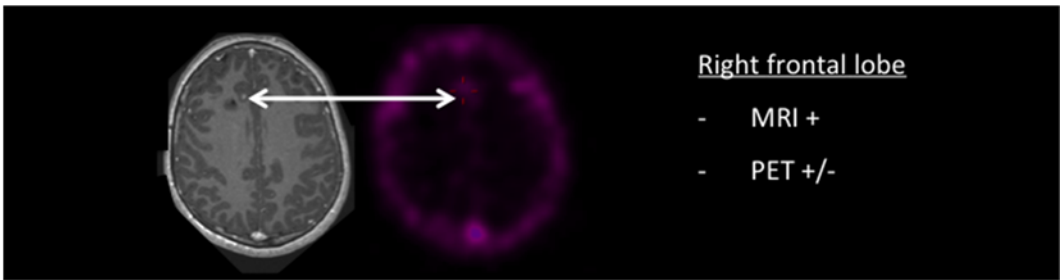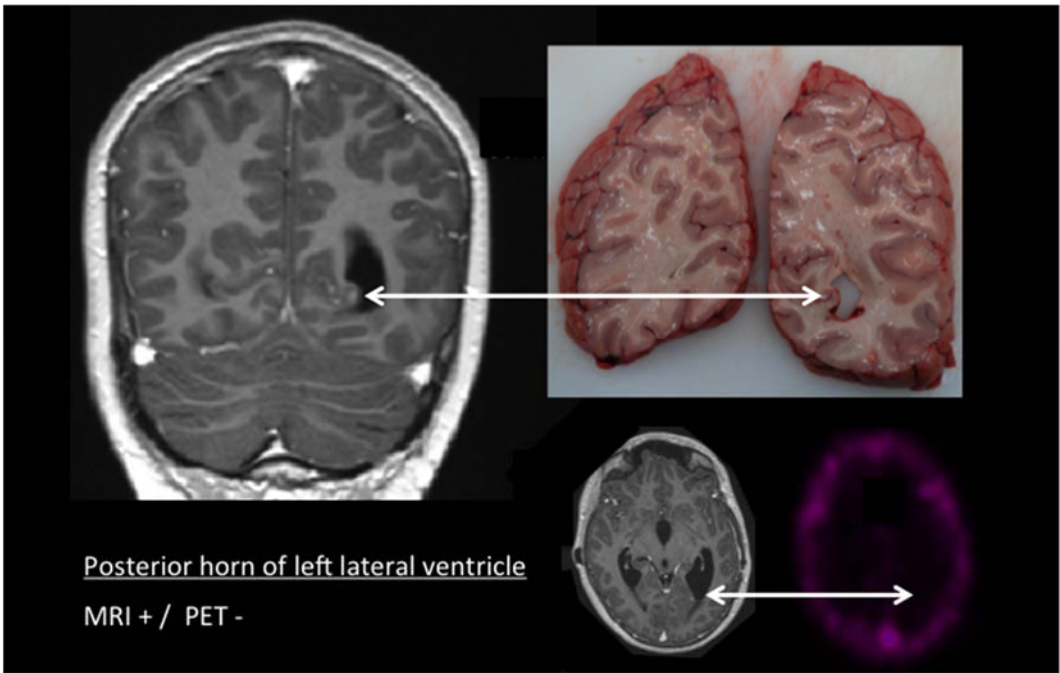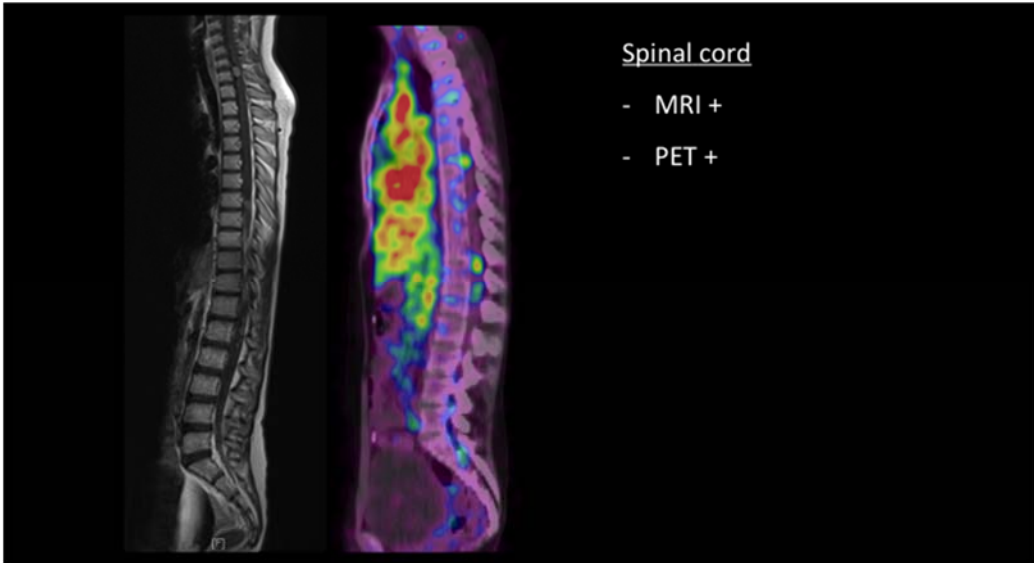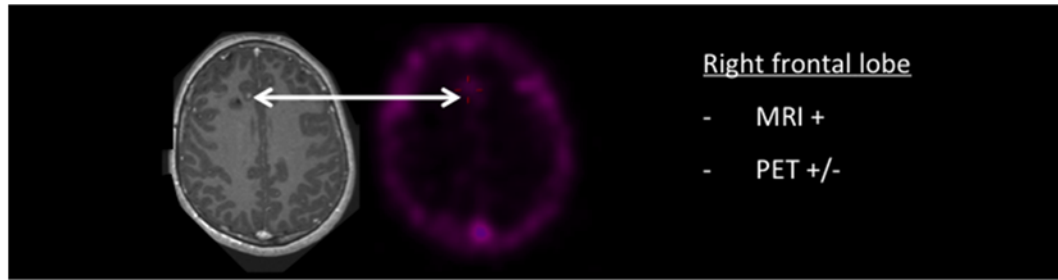
Figure 3. Histology and immunohistochemistry of samples from the cranial and caudal part of the primary pontine tumor and CMM, respectively **(A)** H&E; **(B)** MIB-1 (for detection of proliferating cells); **(C)** astrocyte marker GFAP; **(D)** CD34 (endothelial cell marker) and Glut-1 (a glucose transporter expressed by brain endothelial cells as part of the blood brain barrier, and often deregulated in areas with hypoxia) **(E)** SMA (a marker of vascular smooth muscle cells and activated pericytes) and Coll-IV (a component of

the vascular basal membrane) **(F)** VEGF staining. Original magnification of all images x200. **Note:** the diffuse growth pattern in all samples; extensive necrosis and glomerular microvascular proliferation with multiple MIB-1 positive (endothelial) cells in the microvascular walls in the caudal CMM; partial loss of CD-34 in the caudal pons; similar staining against GFAP, GLUT-1, VEGF in all samples; all (micro)vessels highlighted in the stain against collagen-IV and SMA.
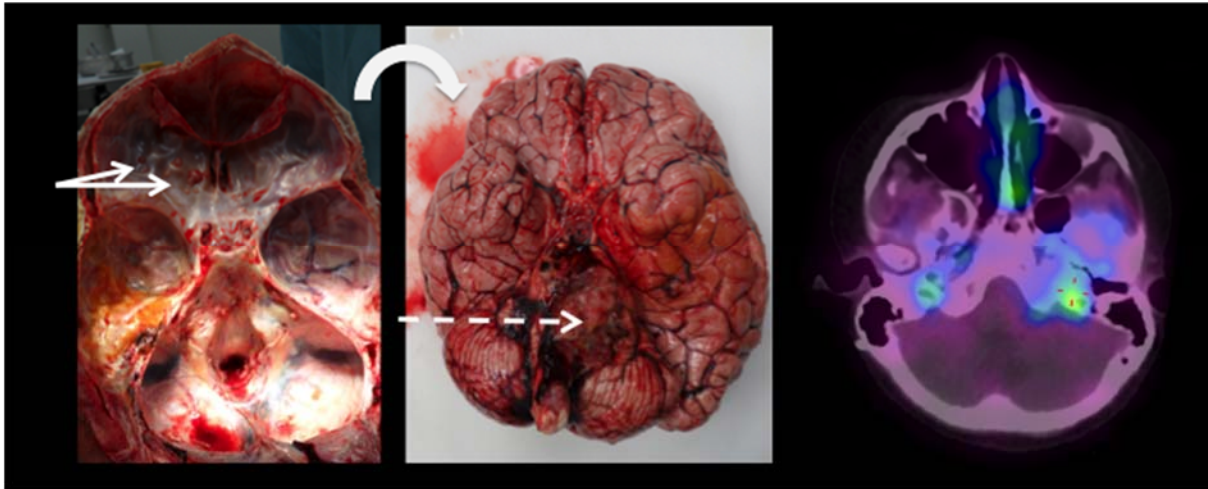
SUPPLEMENTAL DATA

Primary pontine tumor
MRI + / PET +

Cervicomedullary junction
MRI + / PET +

Spinal cord
- MRI +
- PET +

Posterior horn of left lateral ventricle
MRI + / PET -

Right frontal lobe
- MRI +
- PET +/-

Supplemental Figure 1. Gadolinium-enhanced T1-MRI, PET and macroscopy (if available) images of (A) the primary pontine tumor and metastases at the (B) cervicomedullary junction, (C) spinal cord, (D) posterior horn of the left lateral ventricle, (E) right frontal lobe and (F) left Sylvian fissure. White arrows represent areas of ^{89}Zr-bevacizumab uptake and/or disease.

Supplemental Figure 2. Macroscopic picture of the dural metastases (white arrows), which were detected during autopsy but were undetected by MRI and PET. The dotted arrow indicates the primary pontine tumor.